Biomaterials Science

ROYAL SOCIETY OF CHEMISTRY

PAPER

View Article Online
View Journal | View Issue

Cite this: *Biomater. Sci.*, 2023, **11**, 4602

Functionalization of 3D printed polymeric bioresorbable stents with a dual cell-adhesive peptidic platform combining RGDS and YIGSR sequences†

Victor Chausse, [a,b,c] Carlos Mas-Moruno, [a,b,c] Helena Martin-Gómez, [a,b,c] Marc Pino, [d] Maribel Díaz-Ricart, [d] Ginés Escolar, [d] Maria-Pau Ginebra [a,b,e] and Marta Pegueroles* [a,b,c]

Biomimetic surface modification with cell-adhesive peptides is a promising approach to improve endothelialization of current bioresorbable stents (BRS). Among them, RGDS and YIGSR sequences have been reported to mediate adhesion and migration of endothelial cells (ECs) while preventing platelet activation. This work presents the functionalization of novel 3D-printed poly-L-lactic acid (PLLA) and poly(L-lactic-*co*-ε-caprolactone) (PLCL) BRS with linear RGDS and YIGSR sequences, as well as a dual platform (PF) containing both motifs within a single biomolecule. Functionalized surfaces were characterized in terms of static contact angle, biomolecule distribution under confocal fluorescence microscopy and peptide quantification *via* detachment from the surface, showing a biomolecule density in the range of 0.5 to 3.5 nmol cm^{-2}. Biological evaluation comprised a cell adhesion test on functionalized films with ECs and a blood perfusion assay on functionalized stents to assess ECs response and device hemocompatibility, respectively. Cell adhesion assays evidenced significantly increased cell number and spreading onto functionalized films with respect to control samples. Regarding stents' hemocompatibility, platelet adhesion onto PLCL stents was severely decreased with respect to PLLA. In addition, functionalization with RGDS, YIGSR and the PF rendered BRS stents displaying even further reduced platelet adhesion. In conclusion, the combination of intrinsically less prothrombogenic materials such as PLCL and its functionalization with EC-discriminating adhesive biomolecules paves the way for a new generation of BRS based on accelerated re-endothelialization approaches.

Received 15th March 2023,
Accepted 30th April 2023

DOI: 10.1039/d3bm00458a

rsc.li/biomaterials-science

1 Introduction

Stent deployment in stenosed coronary arteries allows for blood flow restoration at the expense of endothelium disruption. Although materials used for stent fabrication are globally biocompatible, their permanent presence in the artery together with the lack of a healthy protective endothelium may lead to adverse biological effects.[1] Metals surface electrical charge and wettability influence protein adsorption behavior in such a way that protein denaturation may occur, which in turn eventually leads to coagulation and thrombosis. Polymer-coated stents are mainly hydrophobic and delaminate as they degrade, leaving the underlying metal exposed.[2] Drug-eluting stents are loaded with antiproliferative drugs to avoid overproliferation of smooth muscle cells (SMCs) and potential restenosis. However, these drugs also inhibit endothelial cells (ECs) proliferation and thus have a detrimental effect on the ultimate recovery of a functional endothelium.[3,4] Besides, newly developed bioresorbable stents (BRS) present high strut profiles associated to increased blood flow turbulence and platelet deposition, contributing to a higher risk of device thrombosis.[5–7] Therefore, stents' clinical performance may only be improved by simultaneously discriminating ECs response from that of SMCs and by ensuring device hemocompatibility.

[a]*Biomaterials, Biomechanics and Tissue Engineering Group, Department of Materials Science and Engineering, and Research Centre for Biomedical Engineering (CREB), Universitat Politècnica de Catalunya (UPC), EEBE, Av. Eduard Maristany, 10-14, 08019 Barcelona, Spain. E-mail: marta.pegueroles@upc.edu; Tel: +34 934054154*
[b]*Barcelona Research Center in Multiscale Science and Engineering, UPC, Eduard Maristany, 10-14, 08019 Barcelona, Spain*
[c]*Institut de Recerca Sant Joan de Déu, Santa Rosa 39-57, 08950 Esplugues de Llobregat, Spain*
[d]*Hematopathology, Pathology Department, Centre de Diagnòstic Biomèdic, Institut d'Investigacions Biomèdiques August Pi i Sunyer, Hospital Clínic, Universitat de Barcelona, 08036 Barcelona, Spain*
[e]*Institute for Bioengineering of Catalonia (IBEC), 08028 Barcelona, Spain*
† Electronic supplementary information (ESI) available. See DOI: https://doi.org/10.1039/d3bm00458a

Accordingly, surface modification of stents has been proposed with the purpose to reduce thrombogenicity, prevent denaturation of adsorbed proteins and accelerate re-endothelialization. Some designs introduce a layer of polymeric material on the stent surface in order to reduce undesirable protein adhesion such as fibrinogen, which may lead to activation of platelets.[1] These coatings can be deposited by means of nonthermal plasma, an extensively used technique for surface activation or modification.[8] For instance, antifouling coatings based on polyethylene glycol (PEG) significantly prevent platelet adhesion.[9–11] Other strategies involve the use of polydopamine (PDA) and polyethylenimine (PEI) as intermediates to incorporate an anti-platelet and anti-thrombotic drug[12] or an anticoagulant drug such as heparin.[13,14] Similarly, Meng *et al.*[15] applied a layer-by-layer strategy to coat 316L stainless steel coronary stents with chitosan and heparin to accelerate re-endothelialization after coronary stent deployment. Alternatively, titanium oxide films have been reported as a suitable coating to improve endothelialization.[16,17] Other authors have followed a different strategy by analyzing the effect of topography on platelet adhesion onto titanium,[18] poly (lactic-*co*-glycolic acid)[19] or cobalt–chromium.[20]

Another approach to achieving hemocompatibility of stents is to functionalize their surface with active biological agents such as nitric oxide (NO) donors, antibodies, growth factors or proteins.[4,21–23] NO plays a key role in vascular biology, as it inhibits the adhesion of platelets and leukocytes, reduces SMCs proliferation and their synthesis of collagen.[24–26] Antibodies have particular potential to accelerate re-endothelialization by capturing circulating endothelial progenitor cells (EPCs) to immobilize them on the stent surface.[27] However, although CD34-binding antibodies capture EPCs from the circulation, no surface marker is unique for EPCs or ECs identification and capture. Lee *et al.* reported a bilayered PCL scaffold functionalized with vascular endothelial growth factor (VEGF) to increase ECs proliferation.[28] Regarding proteins, collagen and fibronectin are two extracellular matrix (ECM) proteins known to enhance ECs attachment and proliferation. However, despite having favorable endothelial cell interactions, both collagen and fibronectin are known to be prothrombogenic and also promote SMCs migration.[2] Conversely, tropoelastin (TE) has shown to have favorable interactions with ECs, low thrombogenicity and growth inhibition of SMCs *in vitro*.[2] Nevertheless, the use of proteins may be troublesome, as it is associated to enzymatic instability, immunogenicity, inflammation risk and high costs.[29]

In this regard, the use of custom-made bioadhesive peptides, which are derived from ECM proteins but encompass only defined cell adhesive motifs, may overcome these limitations and efficiently enhance cell adhesion and improve biointegration *in vitro* and *in vivo*.[29] Bioactive cell-adhesive peptides can be covalently immobilized on polymeric substrates and other biomaterials, following a plasma treatment to activate carboxylic groups or *via* direct chemisorption.[30,31] Regarding peptide sequences, RGDS (Arg–Gly–Asp–Ser) is a universal cell adhesive recognition motif from fibronectin, but REDV (Arg–Glu–Asp–Val, from fibronectin) and YIGSR (Tyr–Ile–Gly–Ser–Arg, from laminin) sequences specifically mediate adhesion and migration of ECs while preventing SMCs and platelet adhesion.[9,32] Other sequences, such as WKYMVm (Trp–Lys–Tyr–Met–Val–D-Met), are reported to stimulate the proliferation of endothelial colony-forming cells.[33] Interestingly, it has been recently shown that the combination of RGD with REDV and YIGSR enhances endothelialization of metallic stents[34] and vascular grafts.[35] However, the optimal configuration and surface distribution of the peptides in order to obtain accelerated ECs response is yet to be elucidated. Furthermore, distinct bioactive peptides can be combined in a single biomimetic molecule to exert synergistic or complementary effects on the surface of an implant.[36–38]

This work presents the functionalization of novel 3D-printed polymeric BRS fabricated by solvent-cast direct-write (SC-DW) technique with EC adhesive peptides. Stents have been manufactured with poly-L-lactic acid (PLLA) and poly(L-lactic-*co*-ε-caprolactone) (PLCL). Solid phase peptide synthesis (SPPS) was used to synthesize linear RGDS and YIGSR sequences with PEG as a spacer unit, as well as a dual-peptide platform containing both RGDS and YIGSR motifs. Biomolecule covalent anchorage on stents and solvent-cast films was achieved subsequent to O_2-plasma treatment to activate carboxylic groups. Functionalized surfaces were characterized in terms of static contact angle, biomolecule distribution under confocal fluorescence microscopy and peptide quantification *via* detachment from the surface. Biological evaluation included a cell adhesion test on functionalized films with human umbilical vein endothelial cells (HUVECs) and a thrombogenicity assay on functionalized stents to assess ECs response and device hemocompatibility, respectively.

2 Materials and methods

2.1 Chemicals and materials

Medical grade PLLA (Purasorb® PL 65; inherent viscosity 6.5 dL g^{-1}, M_w = 1 675 000 g mol^{-1}) and PLCL (Purasorb® PLC 9538, 95 : 5 lactic-to-caprolactone molar ratio, 3.8 dL g^{-1}, M_w = 700 000 g mol^{-1}) were purchased from Corbion (Netherlands). Acetonitrile (ACN, Carlo Erba Reagents, Spain) and chloroform (≥99.5%, Sigma-Aldrich, USA) were used as received. 1-Ethyl-3-(3-dimethylaminopropyl)carbodiimide (EDC) and *N*-hydroxysuccinimide (NHS) were purchased from Sigma-Aldrich (USA). All chemicals required for the peptide synthesis, including resins, Fmoc-L-amino acids and coupling reagents, were obtained from Iris Biotech GmbH (Germany) and Sigma-Aldrich (USA).

2.2 Solvent casting of films

PLLA and PLCL pellets were dissolved in chloroform at 3.6% or 4.5% concentration (w/v), respectively, in a dual asymmetric centrifuge (SpeedMixer™, DAC 150.1 FVZ, FlackTek, Germany) at 3500 rpm in 8 runs of 5 min. Resulting mixtures were poured onto a Petri dish and incubated in a chloroform satu-

rated atmosphere at room temperature (RT) for 3 days. Obtained films underwent thermal treatment at 80 °C for 12 hours and were stored in a desiccator until further use.

2.3 3D printing of stents

PLLA and PLCL stents were manufactured by means of SC-DW technique as reported elsewhere.[39] Briefly, dissolution of PLLA or PLCL pellets in chloroform at a 10% or 12.5% ratio (w/v), respectively, rendered printable inks. Tubular printing was achieved by modification of a BCN 3D+ printer (BCN 3D technologies, Spain) *via* substitution of its *y* axis for a 3 mm in diameter rotating mandrel. Stents were printed with a 250 μm nozzle (Optimum® SmoothFlow™, Nordson, USA) following rhombic cell design, 30 mm in length, 3 mm in diameter and number of peaks equal to 10. After printing, stents were cut in half in the longitudinal direction and flattened between two glass slides, subjected to thermal treatment at 80 °C for 12 hours and stored in a desiccator until further use.

2.4 Solid-phase peptide synthesis

The peptidic sequences RGDS and YIGSR and the combined platform RGDS–YIGSR (PF) were manually synthesized as previously reported.[30,31,34,36] Briefly, Fmoc Rink-amide MBHA resin (200 mg, 0.4 mmol g^{-1}) was used as solid support for solid-phase peptide synthesis following the Fmoc/*t*Bu strategy.[40,41] Deprotection steps and washings between couplings were carried out with *N*,*N*-dimethylformamide (DMF) and dichloromethane (DCM). Solvents and soluble reagents were removed using a vacuum filtration system and all reactions and treatments were performed at room temperature. Sequential coupling reactions were carried out with Fmoc-L-amino acids (3 eq.), ethyl 2-cyano-2-(hydroxyimino)acetate (OxymaPure) (3 eq.) and *N*,*N*-diisopropylcarbodiimide (DIC) (3 eq.) in DMF for 60 min and monitored using the Kaiser test. In the case of the PF, the second branch was constructed after Alloc group removal with 3 treatments of $PhSiH_3$ (10 eq.) and $Pd(PPh_3)_4$ (0.1 eq.) in DCM for 15 minutes. Prior to cleavage, the free N-terminus was either acetylated (Ac) or reacted with 5 (6)-carboxyfluorescein (CF) to obtain fluorescent analogues for physicochemical characterization assays.

Reversed-phase analytical high performance liquid chromatography (RP-HPLC) was performed using Shimadzu Prominence XR (Japan) equipped with a LC-20AD pump, a SIL-20AC cooling autosampler, a CTO-10AS column oven and a SPD-M20A photodiode array detector. A reversed-phase XBridge C18 column (4.6 × 100 mm, 3.5 μm, Waters) was used. The system was run at a flow rate of 1.0 mL min^{-1} over 8 min using water (0.045% trifluoroacetic acid (TFA), v/v) and ACN (0.036% TFA, v/v) as mobile phases. Acetylated peptides were purified by semipreparative RP-HPLC using a Waters modular HPLC System (2545 quaternary gradient module, equipped with a 2489 UV/Vis detector, a 2707 autosampler and a fraction collector III) and a reversed-phase XBridge C18 column (19 × 150 mm, 5 μm, Waters). The system was run at a flow rate of 15 mL min^{-1} over 40 min. The solvents used were water (0.1% TFA, v/v) and ACN (0.05% TFA, v/v). All peptides were characterized by analytical RP-HPLC and matrix-assisted laser desorption/ionization time-of-flight (MALDI-TOF) spectrometry (AB 4800 Plus MALDI TOF/TOF instrument, AB Sciex, Spain). MALDI-TOF spectra and HPLC chromatograms are available in the ESI.† Fig. 1a shows the structure of the synthesized linear peptides and platform.

- **RGD**: Ac–Arg–Gly–Asp–Ser–PEG–PEG–Lys–Lys–NH_2: RP-HPLC (0–40% ACN over 15 min, t_R = 4.335 min, purity 96.2%), MALDI-TOF (*m*/*z* calcd for $C_{41}H_{76}N_{14}O_{16}$, 1021.13; found, 1021.58).
- **CF-RGD**: CF–Arg–Gly–Asp–Ser–PEG–PEG–Lys–Lys–NH_2: RP-HPLC (5–100% ACN over 8 min, t_R = 6.382 min, purity 86.9%), MALDI-TOF (*m*/*z* calcd for $C_{60}H_{84}N_{14}O_{21}$, 1337.39; found, 1338.65).
- **YIGSR**: Ac–Tyr–Ile–Gly–Ser–Arg–PEG–PEG–Lys–Lys–NH_2: RP-HPLC (5–100% ACN over 8 min, t_R = 5.940 min, purity 91.2%), MALDI-TOF (*m*/*z* calcd for $C_{52}H_{91}N_{15}O_{16}$, 1182.37; found, 1182.68).
- **CF-YIGSR**: CF–Tyr–Ile–Gly–Ser–Arg–PEG–PEG–Lys–Lys–NH_2: RP-HPLC (5–100% ACN over 8 min, t_R = 6.918 min, purity 82.5%), MALDI-TOF (*m*/*z* calcd for $C_{71}H_{99}N_{15}O_{21}$, 1498.63; found, 1499.69).
- **RGDS–YIGSR (PF)**: [(Ac–Arg–Gly–Asp–Ser–PEG–PEG)(Ac–Tyr–Ile–Gly–Ser–Arg–PEG–PEG)]–Lys–βAla–Lys–Lys–NH_2: RP-HPLC (5–95% ACN over 3 min, t_R = 1.180 min, purity 93.2%), MALDI-TOF (*m*/*z* calcd for $C_{90}H_{157}N_{27}O_{32}$, 2129.37; found, 2129.16).
- **CF-RGDS–YIGSR (CF-PF)**: [(Ac–Arg–Gly–Asp–Ser–PEG–PEG)(CF–Tyr–Ile–Gly–Ser–Arg–PEG–PEG)]–Lys–βAla–Lys–Lys–NH_2: RP-HPLC (5–100% ACN over 8 min, t_R = 6.714 min, purity 66.3%), MALDI-TOF (*m*/*z* calcd for $C_{109}H_{165}N_{27}O_{37}$, 2445.64; found, 2446.14).

2.5 Surface functionalization

PLLA and PLCL films and stents were O_2-plasma activated for 5 min using a Standard Femto Plasma System (Diener, Germany), as shown in Fig. 1b. Subsequently, O_2-activated samples were treated with 0.1 M EDC and 0.2 M NHS in PBS at pH 6.5 for 2 hours in order to stabilize generated carboxylic groups and render activated esters. In parallel, RGDS and YIGSR linear peptides, and the RGDS–YIGSR platform were dissolved in Milli-Q water at a 100 μM concentration. After rinsing with PBS, a 100 μL drop containing the peptidic molecules was deposited on each sample. The anchorage of the peptides to the surface *via* amide bonds was achieved after incubation overnight at room temperature. Functionalization with fluorescent peptides was performed in the dark. Finally, the excess peptide solution was removed and biofunctionalized films and stents were rinsed thrice with Milli-Q water and dried with N_2 gas until further use.

2.6 Surface physicochemical characterization

The presence and distribution of the peptides was evaluated through contact angle measurements, confocal fluoresce microscopy and biomolecule detachment. Static contact angle was measured with a Contact Angle System OCA15 plus

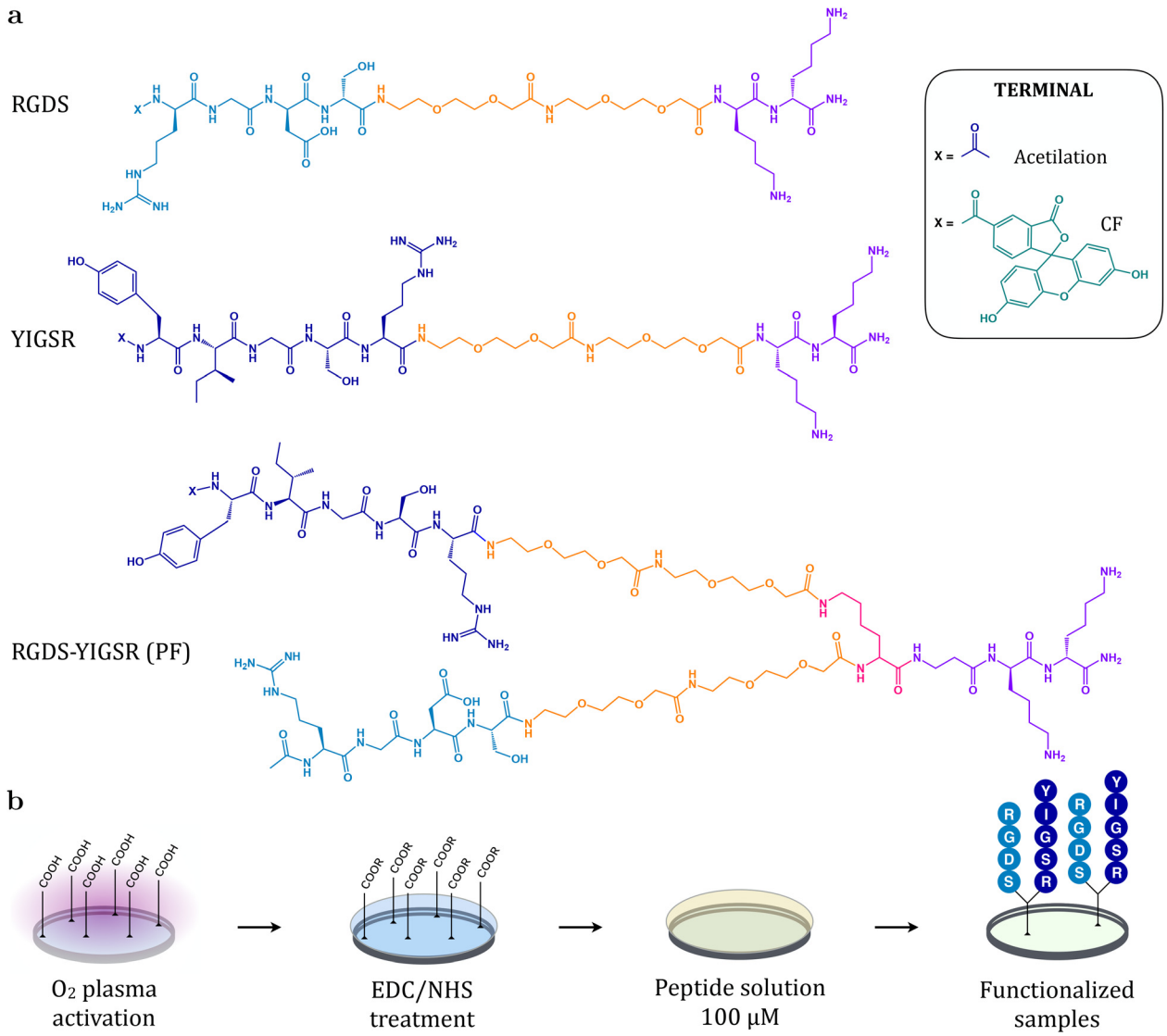

Fig. 1 (a) Chemical structure of the cell adhesive linear peptides and platform. All biomolecules contain the corresponding bioactive sequence (highlighted in blue), two short polyethylene glycol (PEG) chains as a spacing unit (orange) and an anchoring group with two lysine residues (purple). Additionally, the platform presents an extra lysine acting as a branching unit (rose) and a β-alanine as a spacer (black). Finally, all the molecules were either acetylated or reacted with 5(6)-carboxyfluorescein (CF) to obtain fluorescent analogues. (b) Scheme of the functionalization of the PLLA and PLCL films and stents, comprising the activation of the surface with O_2 plasma, the treatment with EDC/NHS and the covalent binding of the biomolecules onto the surface.

(Dataphysics, Filderstadt, Germany) using the sessile drop method. As wetting liquids, Milli-Q water and diiodomethane (CH_2I_2, Acros Organics, Belgium) were used by deposition of a 1 μL drop on functionalized PLLA and PLCL films, with three measurements per sample and three samples per condition. Contact angle values were obtained by application of the Laplace–Young fitting with SCA 20 software (Dataphysics). Surface free energy with partial polar and dispersive components was derived by means of the Owens, Wendt, Rabel, and Kaelble (OWRK) method[42,43] employing the surface tension values for water and diiodomethane determined by Ström *et al.*[44]

Furthermore, functionalized films and stents with carboxyfluorescein-labeled molecules were characterized by means of confocal fluorescence microscopy. The distribution of the peptidic molecules was evaluated in a LSM 800 confocal laser scanning microscope (Carl Zeiss, Germany). Fluorescence intensity was measured by image processing using FIJI software. Additionally, peptide surface density on films and stents was assessed according to a modified protocol described previously.[31] Briefly, functionalized samples with fluorescent peptides were treated in 1 M NaOH solution at 70 °C for 12 minutes in order to detach the biomolecule from the surface. In parallel, a calibration curve of well-known peptidic concentrations, from 125 nM to 20 μM, was performed for each fluorescent molecule. In a 96-well plate with black bottom, 50 μL of the hydrolysate from the samples were

added, as well as of each concentration in the standard curve. Fluorescence intensity was analyzed using a MicroPlate Reader (Synergy HTX multi-mode microplate reader, BioTek Instruments, USA), with $\lambda_{excitation}$ = 485 nm and $\lambda_{emission}$ = 528 nm, and converted to concentration with the corresponding calibration curve.

2.7 Biological characterization

Films and stents functionalized with RGDS and YIGSR linear peptides and the dual platform (PF) containing both motives (RGDS–YIGSR) were evaluated through an adhesion test with HUVECs and a thrombogenicity assay.

2.7.1 HUVECs adhesion test. HUVECs (PromoCell GmbH, Germany) were cultured in endothelial cell growth media (PromoCell, Germany) supplemented with 1% penicillin/streptomycin in Nunc culture flasks (Thermo Fisher Scientific, USA) at 37 °C in a humidified atmosphere with 5% of CO_2. At 90% confluence, cells were detached *via* trypsinization (trypsin/EDTA, Sigma-Aldrich, USA) for 2 min, rinsed with PBS and resuspended in cell medium supplemented with 10% fetal bovine serum (FBS) for trypsin neutralization. Lastly, cells were centrifuged at 220*g* and resuspended in serum-free cell media. All experiments were conducted at passages 7 to 9. In parallel, control PLLA and PLCL films measuring 1 × 1 cm, as well as functionalized films with RGDS, YIGSR and PF, were placed in a low attachment 24 well-plate (Thermo Fisher Scientific, USA) and treated with 1% bovine serum albumin (BSA) in PBS for 30 min. After rinsing three times with PBS, HUVECs were seeded at a density of 20 000 cells per film in serum-free medium. After 6 hours of incubation, non-adherent cells were removed by rinsing twice with PBS. Adhered cells were then fixed with 4% paraformaldehyde (PFA, Sigma Aldrich, USA) in PBS.

Subsequently, immunofluorescent staining was performed to assess the efficiency of the biofunctionalization of the films. After a permeabilization treatment with 0.05% Triton X-100 (Sigma-Aldrich, USA) in PBS for 20 min, cytoskeletal actin filaments (F-actin) were stained using phalloidin (1 : 400) (Invitrogen, USA) in Triton 0.05% for 1 h and nuclei with 4′,6-diamidino-2-phenyldole (DAPI) (1 : 1000) (Life Technologies, USA) in PBS–glycine for 2 min. Washing between treatments was conducted with 20 nM glycine (Sigma-Aldrich, USA) in PBS (3 × 5 min) and both staining steps were performed in the dark. Finally, samples were mounted on microscope slides with Mowiol (Sigma-Aldrich, USA) and observed in a LSM 800 confocal laser scanning microscope (Carl Zeiss, Germany). FIJI software was used to count the number of cells as well as to assess cell spreading by computing their area.

2.7.2 Blood perfusion assay. Stents' hemocompatibility was evaluated in a flat chamber perfusion system as described elsewhere.[20,45] In short, whole blood was obtained from a healthy volunteer and minimally anticoagulated with a citrate/phosphate/dextrose solution at a final citrate concentration of 19 mM (100 mM sodium citrate, 16 mM citric acid, 18 mM sodium hydrogen phosphate, and 130 mM dextrose). Blood was circulated through the perfusion chamber at a shear rate of 800 s^{-1} during 5 min at 37 °C, as shown in Fig. 2. Control and functionalized flattened PLLA and PLCL stents were placed in the chamber aligned with the blood flow (Fig. 2b).

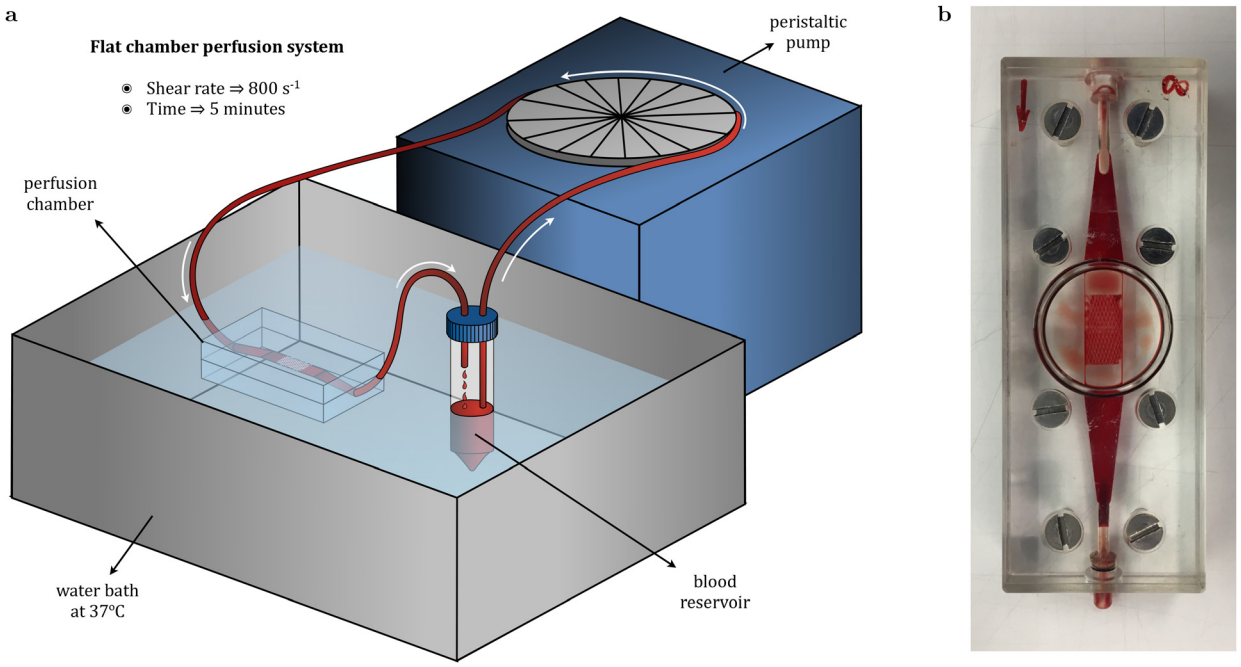

Fig. 2 (a) Scheme showing the experimental setup used for the thrombogenicity assay. Blood from a healthy donor was circulated through the stent in the perfusion chamber at a shear rate of 800 s^{-1} for 5 minutes using a peristaltic pump. Both the blood reservoir and the perfusion chamber were maintained in a water bath at 37 °C. (b) Detail of the perfusion chamber after the assay, with the stent aligned with the blood flow.

After perfusion, stents were rinsed in PBS and adhered platelets were fixed with 2.5% glutaraldehyde in PBS at 4 °C during 24 h. Immunofluorescent staining was performed by a blocking step with 1% BSA in PBS for 30 min, primary antibody monoclonal mouse antihuman CD36 (1 : 2000) (Clone 185-1G2, Lifespan, Biosciences, USA) incubation with 1% BSA in PBS for 1 h, PBS washing (3 × 5 min) and secondary antibody goat antimouse IgG-AF 568 (1 : 500) incubation with 1% BSA in PBS for 1 h in the dark. Finally, stents were washed with PBS and mounted on microscope slides with Mowiol (Sigma-Aldrich, USA) and observed in a LSM 800 confocal laser scanning microscope (Carl Zeiss, Germany). The percentage of the surface covered by platelets was analyzed with FIJI software. The study protocol was approved by the Ethics Committee of the Hospital Clínic and the study complied with all local regulations and the ethical principles of the current Declaration of Helsinki. Informed consent was obtained from the human participant of this study.

Lastly, platelet aggregates were analyzed under scanning electron microscopy (SEM). On that account, platelets were fixed with 2.5% glutaraldehyde in PBS for 30 min and dehydrated through immersion in ethanol : water solutions with increasing ethanol content (30%, 50%, 70%, 90% and 100%) for 10 minutes each. Dehydrated samples were sputtered with platinum–palladium (80 : 20) and examined using JEOL JSM-7001F (JEOL, Japan) at 2 kV acceleration voltage.

2.8 Statistical analysis

Statistical analysis was performed using Minitab software (Minitab Inc., USA). An equality of variances test (ANOVA) with Fisher *post hoc* test was used to determine statistically significant differences ($p < 0.05$ between the different groups and 95% confidence interval) for normally-distributed data. All data are represented as mean values ± standard deviation (SD).

3 Results and discussion

3.1 Biomolecules design and synthesis

The peptidic sequences RGDS and YIGSR and the combined platform (PF) were synthesized following SPPS protocols. Fig. 3 presents a summary of the key synthetic steps to assemble the dual platform. Starting from Fmoc Rink-amide MBHA resin as a solid support, two lysine residues (Lys, labelled purple) were introduced as an anchoring unit. Lysine was chosen for its ability to form stable amide bonds with the carboxylic groups of the polymer activated surface owing to the presence of a primary amine in its side chain. In a second step, an orthogonally protected (Fmoc/Alloc) lysine (Lys, labelled rose) was coupled to act as a branching unit. Under basic conditions, the Fmoc group protecting the α-amine may be selectively removed whereas the Alloc group remains in place, therefore permitting to assemble the next unit exclusively at the α-position. On that account, two short polyethylene glycol (PEG, labelled orange) chains and the first motif (RGDS, labelled sky blue) were coupled. PEG chains act as a spacing unit by providing the necessary separation between the surface and the bioactive sequence, therefore allowing for the optimal accessibility to cell receptors.[34,36,46] Furthermore, it has been shown that PEG possesses an antifouling character, such that unspecific adsorption of proteins and cells is diminished, thus limiting the aggregation of platelets and the risk of potential thrombosis.[10,11,47,48] The second branch with the PEG spacer and the YIGSR motif (labelled dark blue) was introduced after removal of the Alloc group protecting the ε-amine in the branching lysine by means of catalytic amounts of palladium. Finally, the resulting molecule was cleaved from the solid support with concurrent removal of all protective groups in the side chains (*t*Bu, Boc and Pbf), purified and characterized as detailed in the Methods section.

3.2 Peptide immobilization on films and stents

PLLA and PLCL films were successfully obtained through solvent casting. Subsequent to surface O_2-plasma activation, the linear peptides RGDS and YIGSR and the dual PF were covalently anchored onto the films. Table 1 summarizes the data gathered from the static contact angle assay. Plain PLLA presented the highest water contact angle, 94.3° ± 3.6, whereas plain PLCL exhibited a marginally more hydrophilic behavior with 83.1° ± 5.1 ($p < 0.05$). When functionalizing the polymers with RGDS, YIGSR or the PF the contact angle decreased to around 60° independently of the base material, with differences among biomolecules found to be statistically non-significant. A decrease in the water contact angle is widely described in the literature after application of plasma treatments to PLLA[49–51] or subsequent to grafting with RGDS and YIGSR peptides.[34,52] Regarding surface free energy (γ), PLLA was found to present the lowest among all conditions, specially with almost negligible polar component (γ^p). Analogously to increasing hydrophilicity when functionalized, PLLA and PLCL's surface free energy also increased to around 55 mJ m^{-2}, both in terms of dispersive and polar components.

In order to assess the spatial distribution of the biomolecules, PLLA and PLCL films were functionalized with their fluorescent analogues. Fig. 4a shows overview images of the films obtained under confocal fluorescence microscopy, which evidenced the homogeneity of the grafting throughout the totality of the surface, although with the sparse presence of peptidic aggregates. A semiquantitative analysis of the fluorescence intensity displayed by the films is shown in Fig. 4b. In general, increased fluorescence intensity was found for CF-PF when compared to CF-RGDS, with no striking differences between PLLA and PLCL conditions.

Analogously, 3D-printed PLLA and PLCL stents were functionalized with the synthesized biomolecules in their fluorescent version. Fig. 5a presents the spatial distribution of peptides on PLLA and PLCL flattened stents, covering the entirety of the stent struts. Although the stents were successfully coated in a homogenous fashion, peptide agglomerates were detected at some strut junctions, such as for PLLA functionalized with CF-YIGSR. Regarding fluorescence intensity analysis, a similar trend to the one observed for functionalized films

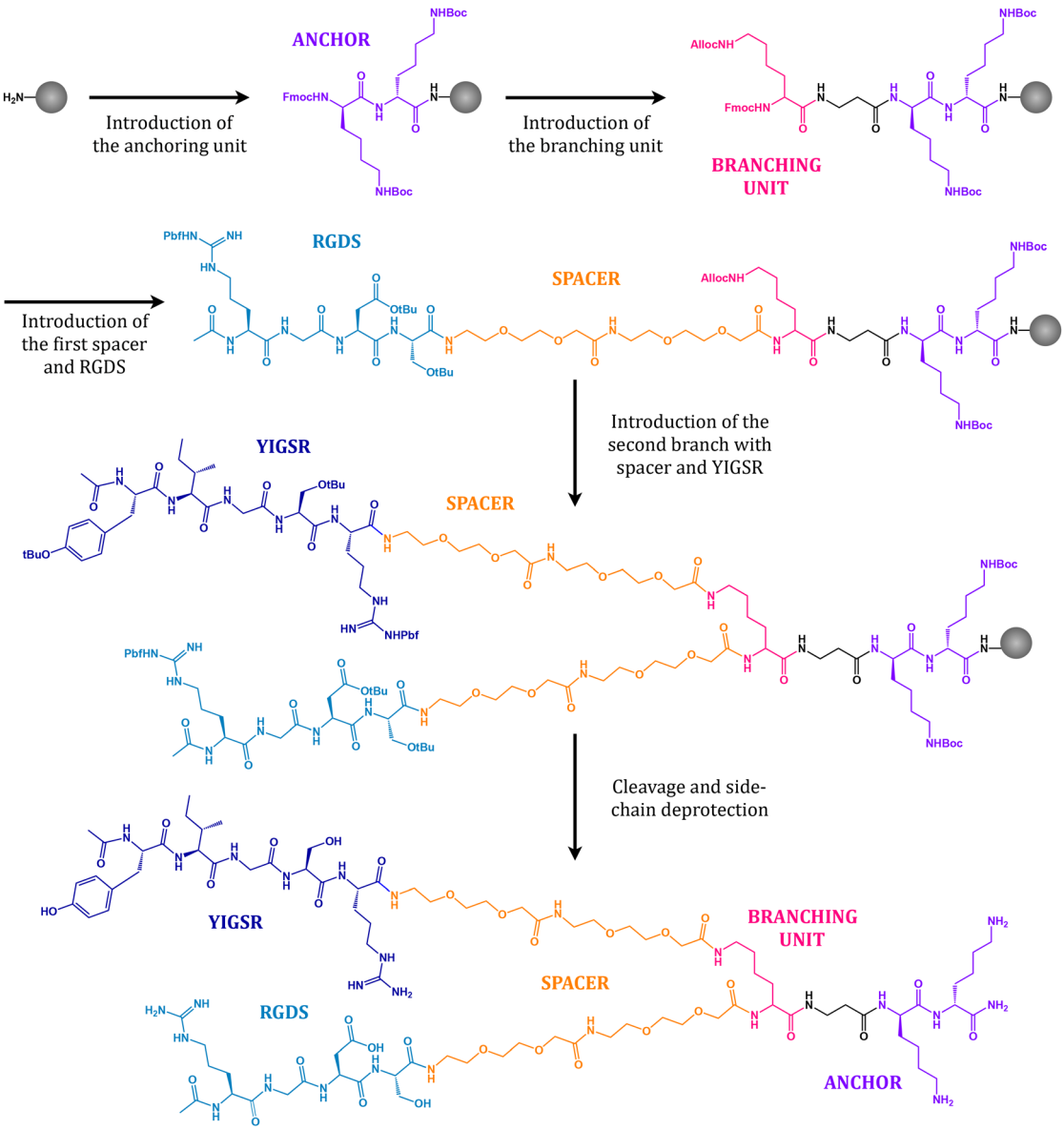

Fig. 3 Main steps during the synthesis of the dual platform. The major components are highlighted in color: the anchor (purple), branching (rose) and spacer (orange) units, the RGDS motif (sky blue) and the YIGSR motif (dark blue).

Table 1 Physicochemical characterization of PLLA and PLCL films functionalized with RGDS, YIGSR and PF with respect to control. Static contact angle for water (θ_{H_2O}), diiodomethane ($\theta_{CH_2I_2}$) and total surface free energy (γ), split in dispersive component (γ^d) and polar component (γ^p). Conditions a–d are statistically different ($p < 0.05$) for each variable

Sample		Contact angle [°]		Surface free energy [mJ m^{-2}]		
		θ_{H_2O}	$\theta_{CH_2I_2}$	γ	γ^d	γ^p
PLLA	Control	94.3 ± 3.6^a	44.7 ± 4.4^a	37.7 ± 1.6^a	37.2 ± 2.0^a	0.6 ± 0.4^a
	RGDS	62.3 ± 4.1^d	27.6 ± 5.1^b	54.6 ± 2.3^b	45.1 ± 1.9^b	9.5 ± 0.6^c
	YIGSR	59.8 ± 6.7^d	22.2 ± 9.1^b	56.9 ± 4.3^b	46.7 ± 3.4^b	10.2 ± 1.9^c
	PF	67.5 ± 5.5^c	24.4 ± 5.0^b	53.1 ± 2.8^b	46.3 ± 1.4^b	6.8 ± 1.5^{b,c}
PLCL	Control	83.1 ± 5.1^b	44.9 ± 2.5^a	40.1 ± 2.0^a	37.0 ± 2.0^a	3.1 ± 1.2^{a,b}
	RGDS	59.5 ± 6.3^d	28.8 ± 9.6^b	55.5 ± 5.3^b	44.4 ± 3.5^b	11.1 ± 2.0^c
	YIGSR	63.2 ± 7.0^{c,d}	29.1 ± 6.3^b	53.8 ± 2.7^b	44.5 ± 1.3^b	9.3 ± 2.8^c
	PF	58.6 ± 2.9^d	29.4 ± 6.3^b	55.9 ± 2.4^b	44.3 ± 2.7^b	11.6 ± 1.3^c

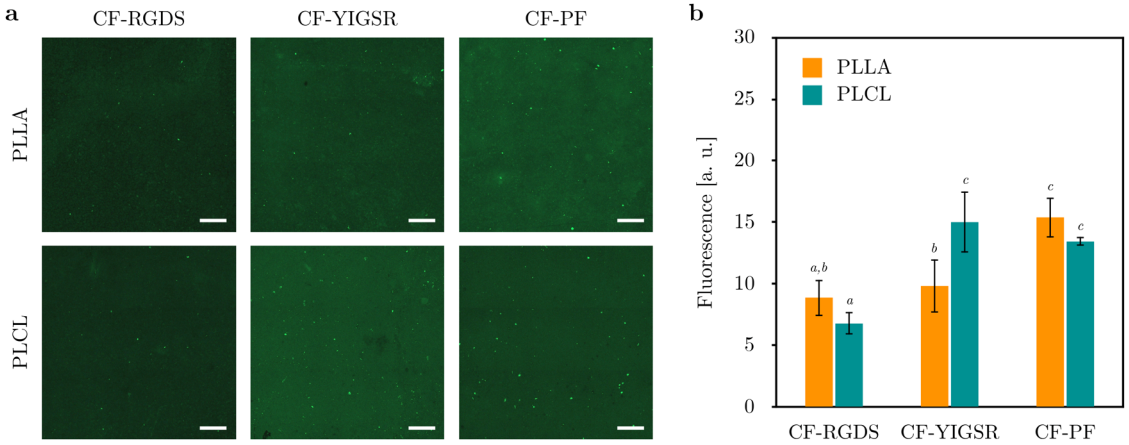

Fig. 4 (a) Spatial distribution of the linear sequences RGDS and YIGSR and the dual PF combining both motifs labelled with 5(6)-carboxyfluorescein (CF) onto PLLA and PLCL films under confocal fluorescence microscopy. Scale bar = 500 μm. (b) Semiquantitative analysis of the absolute fluorescence intensity onto PLLA and PLCL films measured by image processing. Conditions a–c are statistically different ($p < 0.05$).

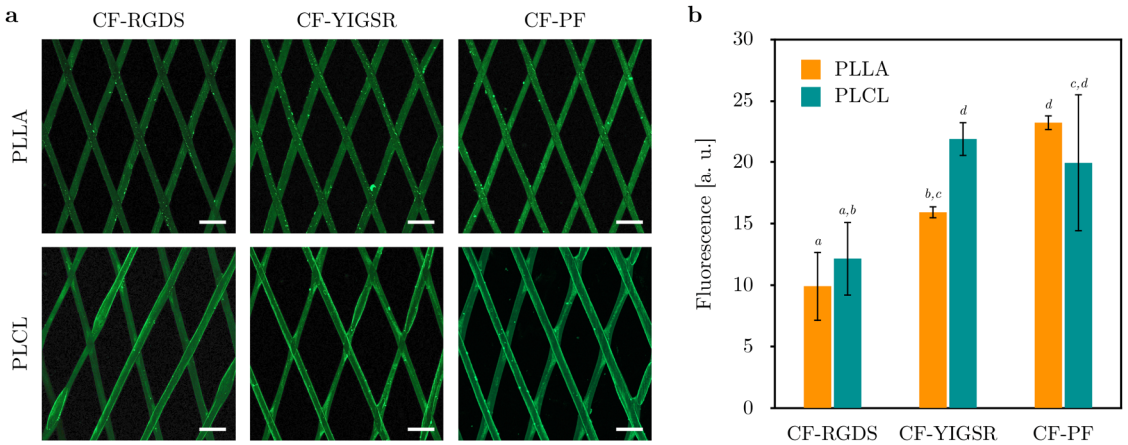

Fig. 5 (a) Spatial distribution of the fluorescent-labeled biomolecules CF-RGDS, CF-YIGSR and CF-PF onto PLLA and PLCL stents under confocal fluorescence microscopy. Scale bar = 500 μm. (b) Semiquantitative analysis of the absolute fluorescence intensity onto PLLA and PLCL stents measured by image processing. Conditions a–d are statistically different ($p < 0.05$).

was found, as shown in Fig. 5b. Stents functionalized with CF-RGDS displayed the lowest fluorescent intensity, whereas those grafted with CF-YIGSR and CF-PF presented significantly higher fluorescence. Furthermore, functionalized stents presented fluorescence intensity values higher than those observed for functionalized films.

Nevertheless, fluorescent intensity values obtained through image processing may be misleading when comparing different types of samples. For instance, films were only functionalized on one of their faces, acting as a two-dimensional object. Conversely, in the case of stents, biomolecule anchorage took place all around the stent struts as a three-dimensional object. Therefore, fluorescent intensity shown by stents may be overestimated due to the integration of the fluorescence readout coming from the different layers in which the stent was sliced.

Consequently, an alternative quantitative method was sought by means of biomolecule detachment. Quantification of the amount of peptide covalently bound to the polymeric substrates was achieved *via* detachment in alkaline conditions through a calibration curve of well-known peptidic concentrations. As shown in Table 2, the peptidic concentration in films was found to be around 500 pmol cm^{-2} for CF-RGDS, 1 nmol cm^{-2} for CF-YIGSR and over 3 nmol cm^{-2} for the dual CF-PF. No differences were found between PLLA and PLCL conditions. In the case of stents, biomolecule density ranged from 0.5 to 3.5 nmol cm^{-2}, with the CF-PF presenting the highest concentration and CF-RGDS the lowest. Again, PLLA and PLCL showed equivalent peptide density.

These results are according to previous works reported in the literature. Aubin *et al.* functionalized decellularized ECM with RGDS and YIGSR linear peptides through physical adsorption, and subsequent quantification of fluorescence intensity showed a slightly higher attachment rate of YIGSR compared to RGDS.[35] Similarly, Oliver *et al.* functionalized glass and titanium substrates through silanization with a dual

Table 2 Biomolecule density onto PLLA and PLCL films and stents quantified *via* biomolecule detachment in 1 M NaOH solution at 70 °C for 12 minutes. Conditions a and b are statistically different ($p < 0.05$)

	Films		Stents	
Biomolecule density [nmol cm^{-2}]	PLLA	PLCL	PLLA	PLCL
CF-RGDS	0.58 ± 0.19^{a}	0.57 ± 0.09^{a}	0.47 ± 0.01^{a}	0.51 ± 0.05^{a}
CF-YIGSR	1.01 ± 0.17^{a}	1.10 ± 0.23^{a}	0.95 ± 0.05^{a}	1.04 ± 0.05^{a}
CF-PF	3.24 ± 0.37^{b}	3.52 ± 0.33^{b}	2.81 ± 0.52^{b}	3.53 ± 0.44^{b}

platform containing both a cell-adhesive RGDS motif and a osteogenic DWIVA sequence (Asp–Trp–Ile–Val–Ala).[31] Following detachment of the fluorescent peptide and quantification with a standard curve, peptide density was found to be around 40 pmol cm^{-2} for glass and close to 80 pmol cm^{-2} for titanium. Other studies have used quartz crystal microbalance with dissipation (QCM-D) monitoring to measure peptide density, such as RGDS, REDV and YIGSR linear peptides on CoCr, with peptide density between 30 and 180 pmol cm^{-2}.[34] QCM-D has also been used to measure RGD peptidomimetics or a platform combining both RGD and a lactoferrin-derived antimicrobial peptide on titanium, finding molecule density between 10 and 550 pmol cm^{-2}.[53,54] Noel *et al.* monitored the grafting of RGDS, REDV and YIGSR with PEG on polyvinylamine-coated polyester through absorbance, and obtained peptide density between 20 and 2000 pmol cm^{-2}.[55] Finally, Lei *et al.* estimated RGDS, REDV and YIGSR surface density onto PET *via* fluorescence microscopy, obtaining values as high as 25 nmol cm^{-2}.[52] Overall, the biomolecule density values obtained for PLLA and PLCL films and stents were found to be in the range of those previously reported, albeit dissimilar anchoring strategies and quantification methods were used.

3.3 Cell adhesion

The biological performance of the biomolecules was assessed by means of an adhesion test with HUVECs. Fig. 6a presents cell adhesion onto control and functionalized PLLA and PLCL films, visually showing increased cell number and cell spreading when ECs were incubated onto functionalized samples with respect to control untreated samples. Quantification of cell number and cell area are shown in Fig. 6b and c, respectively. Biomolecule grafting significantly improved the number of adherent ECs to PLLA, in a tendency that was found to be even more pronounced for PLCL. With respect to the different biomolecules, although both RGDS and YIGSR linear sequences showed increased number of adhered cells, the platform (PF) combining both motifs presented the best results. A similar trend was found when analyzing cell spreading. While adhered to the surface, ECs in control samples presented sphere-like shape, whereas when introducing cell-adhesive peptides cells regained a more extended morphology. The condition showing the highest cell area was PLLA functionalized with YIGSR. Still, all biomolecules significantly improved cell spreading in comparison to plain PLLA and PLCL samples.

These results are in agreement with the increased hydrophilicity displayed by the functionalized films. In general, cell adhesion increases with increasing wettability. As reported by Lee *et al.*, cells adhere and spread on surfaces with moderate hydrophilicity, with maximum adhesion and growth found at water contact angles in the range of 50° to 60°.[56] Furthermore, surface free energy constitutes an indicator of potential cellular adhesion, with materials displaying surface energy above 30 mJ m^{-2} tending to present greater bioadhesion.[57] In the case of PLLA, several authors have associated a greater wettability with improved cell adhesion following oxygen or nitrogen plasma treatments.[49,50]

Concerning the use of peptides, a wide variety of studies have reported improved adhesion, proliferation and migration of ECs on different metallic and polymeric materials functionalized with RGDS[46] and/or REDV[34,55,58–62] and/or YIGSR.[9,34,52,63–65] Among them, Castellanos *et al.* compared the effects of CoCr surface functionalization with RGDS, REDV and YIGSR peptides.[34] Cell studies demonstrated that an equimolar combination of RGDS and YIGSR greatly enhanced ECs adhesion and proliferation without significantly enhancing SMCs adhesion. Similar results regarding the combination of RGDS and YIGSR at an equimolar ratio were described in the studies of Peng *et al.*[65] and Choi *et al.*[63] Besides, it had previously been reported that RGDS induced more cell adhesion than YIGSR and REDV,[52] in contrast to the results presented in this work. Nevertheless, this may be explained by the high densities at which the different peptides were grafted on the surface (0.5 to 1 nmol cm^{-2}), as Noel *et al.* demonstrated that, over a certain density threshold, RGDS and YIGSR presented similar performance with regards to HUVECs cell adhesion.[55] Furthermore, it has been indicated that RGDS and YIGSR interact *via* distinct mechanisms with cells, the former through multiple integrins and the latter *via* the 67 kDa laminin receptor, thus with the potential to act synergistically.[52] The results obtained in the present work are therefore in accordance with those presented previously, showing that the inclusion of both peptide motifs in a unique biomolecule suggests the occurrence of synergistic effects in cell adhesion.

3.4 Platelet adhesion

Platelet adhesion was evaluated through a blood perfusion assay by placing the stents in a flat perfusion chamber maintained at 37 °C while donor's blood was pumped at a shear rate of 800 s^{-1} for 5 minutes. Adherent platelets' membrane was labelled with a fluorescent dye in order to visualize platelet adhesion on stent struts under confocal fluorescence microscopy (Fig. 7a). Qualitatively, obtained overview images

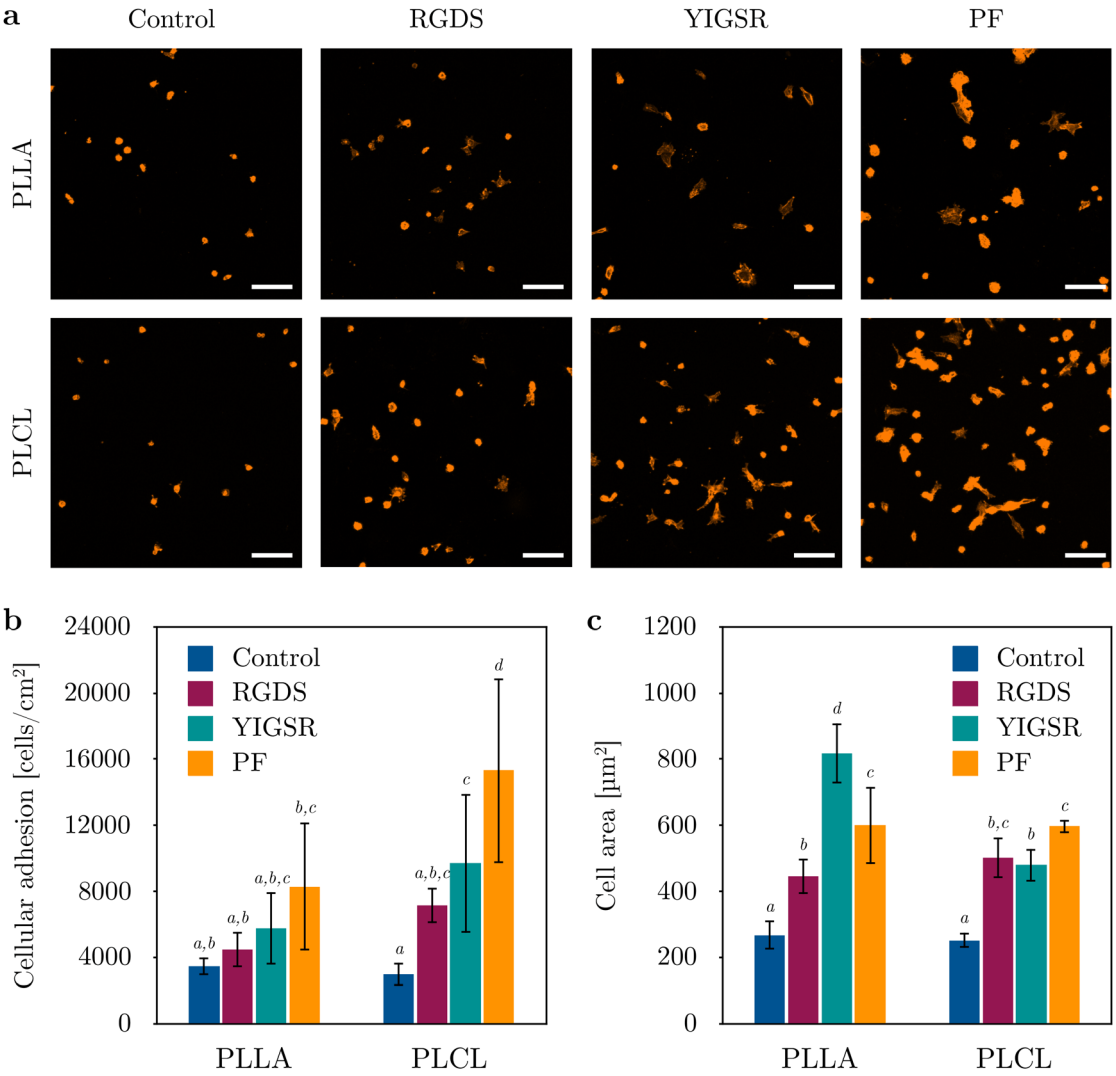

Fig. 6 HUVECs cell adhesion on control and functionalized PLLA and PLCL films after 6 hours of incubation. (a) Confocal fluorescence microscopy images, with actin filaments immunostained with phalloidin. Scale bar = 100 μm. (b) Cell attachment, in cells per cm^2, and (c) cell spreading, in μm^2. Conditions a–d are statistically different ($p < 0.05$).

evidenced the dissimilarities arising among the different conditions. For PLLA, unmodified stents presented significant platelet adhesion, whereas it was found to be much lower for stents functionalized with peptides. Image analysis with FIJI permitted to compute the percentage of stent surface occupied by platelets, showing that for plain PLLA, 28.8% of its area presented adherent platelets (Fig. 7b). In addition, both the linear peptides RGDS and YIGSR, together with the dual PF, presented an antithrombogenic effect, as the area covered by platelets was found to be around or below 5%. Among the biomolecules, RGDS seemed to have the most powerful antithrombogenic effect, although differences with YIGSR and PF were minimal. Conversely, plain PLCL appeared to present a much lower prothrombogenic behavior than plain PLLA, as only 5.2% of its surface was covered by platelets, an equivalent percentage to functionalized PLLA stents. Furthermore, functionalization of PLCL with the biomolecules rendered stents with outstanding hemocompatibility, with platelet coverage found to be around 1% of the stent's surface. This behavior was further confirmed upon sample dehydration and visualization under SEM. As shown in Fig. 7c, platelet aggregates were extensive in control PLLA stents, whereas functionalized samples presented only individual platelets at certain locations. Similarly, platelet adhesion was found to be infrequent for control PLCL stents, and even more sporadic for functionalized stents.

The coagulation cascade that may lead to thrombosis and potential stent failure is triggered by platelet activation, which in turn depends on protein adsorption onto the polymer surface. Activated platelets extend pseudopods and spread over the surface before releasing signals for other platelets that eventually lead to thrombi formation. Therefore, hemocompatibility is mainly driven by the biomaterial's wettability, functional chemical groups availability, charge and topography

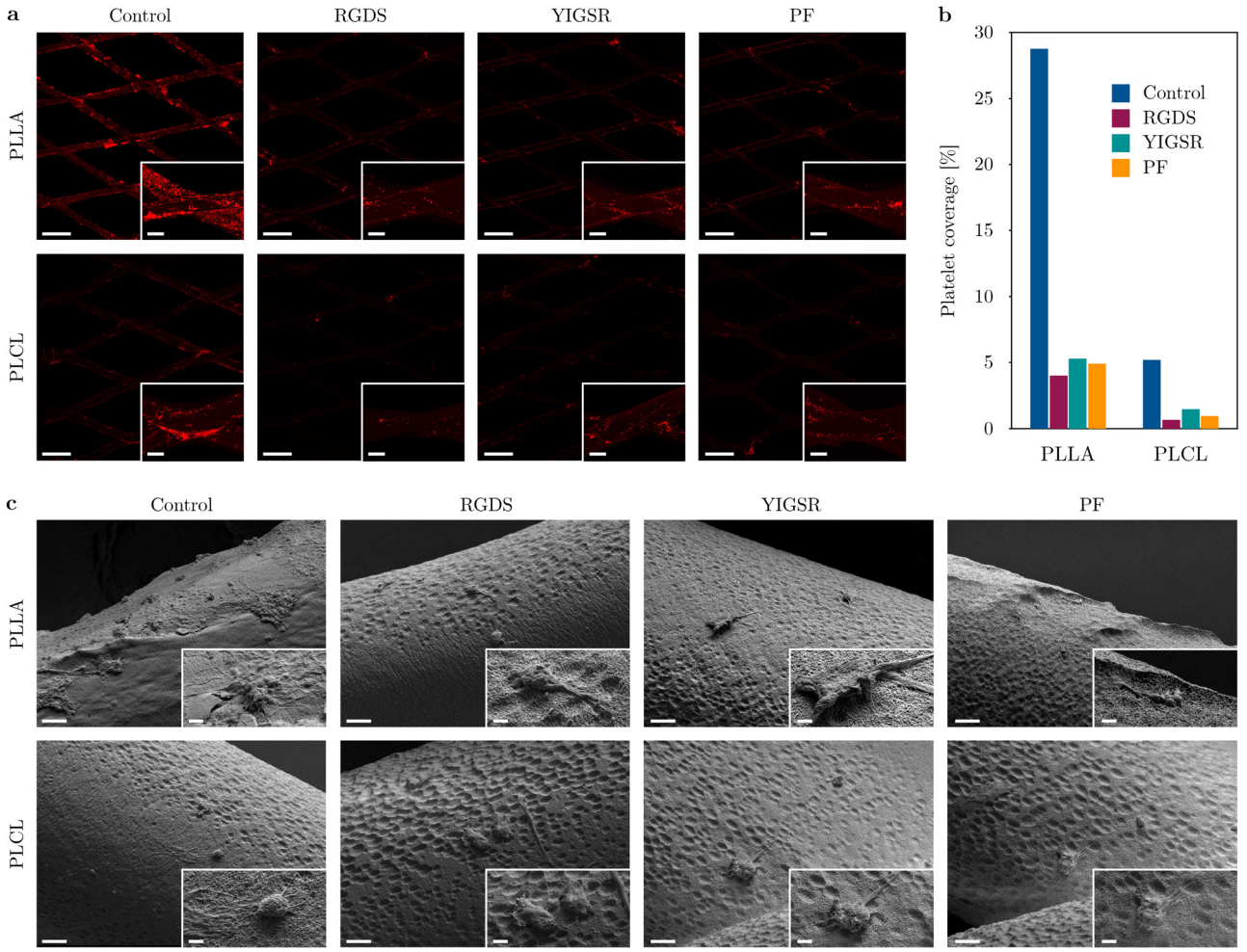

Fig. 7 Platelet adhesion on control and functionalized PLLA and PLCL stents following blood perfusion in a chamber for 5 minutes at a shear rate of 800 s^{-1}. (a) Fluorescence microscopy overview images of adhered platelets on control and functionalized stents (scale bar = 500 μm), with focus on strut junctions (scale bar = 100 μm). (b) Percentage of the stent's area occupied by platelets. (c) SEM images of adherent platelets (scale bar = 10 μm), with magnified details of individual platelets or platelet aggregates (scale bar = 2 μm).

with regards to protein adsorption.[66,67] Among the proteins present in the blood plasma, albumin is regarded as beneficial due to its capacity to generate a passivating layer, whereas adsorption of fibrinogen promotes platelet deposition.[68] Strohbach *et al.* investigated the role of biodegradable PLLA-based polymers in blood cell activation by measuring fibrinogen adsorption. Among the different polymers, PLLA presented the highest fibrinogen adsorption and platelet activation. In general, hydrophobic surfaces facilitate adsorption of proteins and thus platelet-surface activation, whereas in hydrophilic surfaces protein adsorption is impaired due to the energetic cost of displacing water.[69,70] On that account, although PLLA is broadly regarded to be hemocompatible,[71,72] several authors have described strategies to improve its hemocompatibility through surface functionalization.[22,73] Some authors have focused on favouring albumin adsorption over that of fibrinogen by means of PLLA fluorination or have studied the impact that surface chemistry has on adsorbed fibrinogen conformation and its influence on platelet adhesion and activation.[74,75] Other approaches include the loading of drugs such as curcumin and paclitaxel,[76] heparin[77,78] or tantalum ions to improve hydrophilicity.[79] Hietala *et al.* analyzed platelet deposition on stainless steel and PLLA stents, with the latter showing increased platelet adhesion.[13] However, when coating the PLLA stent with a PLCL layer, platelet attachment was effectively reduced. This behavior was also reported by Rudolph *et al.* regarding the thrombogenetic potential of different polymers following a platelet activation test.[80] PLLA was shown to activate platelets in view of high levels of β-thromboglobulin, a protein exerted from platelet granules upon activation, whereas PLCL (70 : 30) presented β-thromboglobulin concentration within the normal range. Similarly, PLLA/PCL blends were found to induce significantly less platelet aggregation than PLLA in a blood cell activation study. Although fibrinogen concentration was comparable to that of PLLA, the authors attributed the dissimilar platelet response to the conformational state of adsorbed fibrinogen.[69] These results are in agreement with the better hemo-

compatibility shown by plain PLCL stents with respect to control PLLA stents (Fig. 7a and b) and with its lower water contact angle (83.1 ± 5.1 *vs.* 94.3 ± 3.6) and higher surface free energy, specially regarding its polar component, as shown in Table 1.

Furthermore, the lower thrombogenicity associated to the presence of peptides has been previously reported for REDV[58–61] and/or for YIGSR.[9,24,55,63,64,81] Although it has been shown that the REDV sequence is recognized by $\alpha_4\beta_1$ integrin receptors, which are hardly present on the platelets surface, the mechanism in which the YIGSR sequence affects platelet adhesion and aggregation is not yet fully understood. Tandon *et al.* had reported that YIGSR supported platelet adhesion through the 67 kDa laminin receptor on platelets.[82] Conversely, Castellanos *et al.* reported that YIGSR and YIGSR + RGD peptides showed decreased platelet adhesion and aggregation, analogously to Peng *et al.*, and suggested that YIGSR might block $\alpha_{IIb}\beta_3$ integrin, that is, the most abundant platelet receptor.[81,83] Hence platelet interaction with laminin remains ill-defined and YIGSR role is still a matter of controversy.[55] Regarding the role of RGDS, Kapp *et al.* evaluated the activity and selectivity profile of ligands for RGD-binding integrins, showing that RGD peptides were active on integrins $\alpha_v\beta_3$, $\alpha_v\beta_5$, $\alpha_5\beta_1$, and selective against $\alpha_v\beta_6$, $\alpha_v\beta_8$ and $\alpha_{IIb}\beta_3$.[84] Therefore, RGDS affinity for platelets would be presumed to be low. Nevertheless, Peng *et al.* found that RGD significantly induced more platelet activation than REDV or YIGSR in silk fibroin scaffolds,[65] whereas Castellanos *et al.* reported that the RGDS coating was the condition with a lower platelet adhesion compared to YIGSR and RGDS + YIGSR.[81] In spite of the aforementioned discrepancies, all biomolecules evaluated in this work displayed similar antithrombogenic behavior.

Altogether, the grafting of biomolecules on hydrophobic polymers such as PLLA appears as a successful strategy for cardiovascular applications. On the one hand, functionalization with peptides resulted in reduced platelet adhesion and activation. On the other hand, peptide sequences such as YIGSR, specifically targeting ECs, effectively improved cell adhesion and spreading. In addition, its combination with RGDS in a single dual molecule evinces the synergistic effects that such an engineered biomolecule may foster in the full endothelialization of a bioresorbable stent.

4 Conclusions

In this work we have presented the functionalization of novel 3D-printed PLLA and PLCL BRS with endothelial cell adhesive peptides to enhance ECs response and stents' hemocompatibility. Linear sequence RGDS and YIGSR peptides have been synthesized, as well as a dual platform presenting both motifs in a single biomolecule. Successful functionalization of films and stents has been confirmed upon water angle measurements and confocal fluorescence microscopy. Quantification of covalently-bond peptides has been achieved by detachment in alkaline conditions, yielding biomolecule density in the range of 0.5 to 3.5 nmol cm^{-2}. Cell adhesion assays evidenced significantly increased cell number and spreading onto functionalized films with respect to control samples. The inclusion of RGDS and YIGSR in a unique platform suggested the occurrence of synergistic effects. Stents' hemocompatibility was evaluated upon a blood perfusion assay, with PLCL showing pronouncedly diminished platelet adhesion with reference to PLLA. In addition, functionalization with RGDS, YIGSR and the PF rendered BRS displaying even further reduced platelet adhesion.

The conjunction of intrinsically less prothrombogenic materials such as PLCL and its functionalization with cell adhesive peptides constitutes an encouraging approach in the treatment of coronary heart disease. The fact that YIGSR and the dual PF simultaneously increase cell adhesion while reducing platelet activation paves the way for a new generation in BRS development. Furthermore, BRS loaded with antiproliferative drugs to avoid restenosis due to overproliferation of SMCs may be functionalized with ECs-discriminating adhesive sequences in order to guide EC proliferation until complete re-endothelialization of the scaffold.

Author contributions

Victor Chausse: conceptualization, investigation, methodology, validation, writing – original draft. Carlos Mas-Moruno: conceptualization, methodology, writing – review & editing. Helena Martin-Gómez: investigation, methodology. Marc Pino: investigation, methodology. Maribel Díaz-Ricart: methodology, writing – review & editing, funding acquisition. Ginés Escolar: supervision, funding acquisition. Maria Pau-Ginebra: supervision, funding acquisition. Marta Pegueroles: conceptualization, formal analysis, writing – review & editing, supervision, methodology, funding acquisition.

Conflicts of interest

There are no conflicts of interest to declare.

Acknowledgements

Financial support was received from the Agency for Administration of University and Research Grants (AGAUR) of the Generalitat de Catalunya (2021SGR-01368, 2021-SGR-01118) and from the Spanish Government, MCIN/AEI/10.13039/501100011033/FEDER (PID2021-124868OB-C22, PID2020-114019RBI00). This work was supported by the project BASE3D 001-P-001646, co-financed by the European Union Regional Development Fund within the framework of the ERDF Operational Program of Catalonia 2014–2020. V. C. thanks the Generalitat de Catalunya for the 2019FI-B00627 scholarship. Support for the research of M.-P. G. was received through the prize "ICREA Academia" for excellence in research, funded by the Generalitat de Catalunya. The authors

also express their gratitude to Javier Valle and David Andreu for their assistance regarding peptide purification.

Notes and references

1 A. Foerster, M. Duda, H. Kraśkiewicz, M. Wawrzyńska, H. Podbielska and M. Kopaczyńska, *Functionalised Cardiovascular Stents*, Elsevier, 2018, pp. 137–148.
2 M. Santos, A. Waterhouse, B. Lee, A. Chan, R. Tan, P. Michael, E. Filipe, J. Hung, S. Wise and M. Bilek, *Functionalised Cardiovascular Stents*, Elsevier, 2018, pp. 211–228.
3 T. J. Parry, R. Brosius, R. Thyagarajan, D. Carter, D. Argentieri, R. Falotico and J. Siekierka, *Eur. J. Pharmacol.*, 2005, **524**, 19–29.
4 P. Qi, S. Chen, T. Liu, J. Chen, Z. Yang, Y. Weng, J. Chen, J. Wang, M. F. Maitz and N. Huang, *Biointerphases*, 2014, **9**, 029017.
5 K. Kolandaivelu, R. Swaminathan, W. J. Gibson, V. B. Kolachalama, K.-L. Nguyen-Ehrenreich, V. L. Giddings, L. Coleman, G. K. Wong and E. R. Edelman, *Circulation*, 2011, **123**, 1400–1409.
6 Y. Sotomi, Y. Onuma, C. Collet, E. Tenekecioglu, R. Virmani, N. S. Kleiman and P. W. Serruys, *Circ. Res.*, 2017, **120**, 1341–1352.
7 E. Tenekecioglu, Y. Sotomi, R. Torii, C. Bourantas, Y. Miyazaki, C. Collet, T. Crake, S. Su, Y. Onuma and P. W. Serruys, *Int. J. Cardiovasc. Imaging*, 2017, **33**, 1313–1322.
8 M. Ramkumar, P. Cools, A. Arunkumar, N. De Geyter, R. Morent, V. Kumar, S. Udaykumar, P. Gopinath, S. Jaganathan and K. Pandiyaraj, *Functionalised Cardiovascular Stents*, Elsevier, 2018, pp. 155–198.
9 H.-W. Jun and J. L. West, *J. Biomed. Mater. Res., Part B*, 2005, **72**, 131–139.
10 J.-k. Park, D.-G. Kim, I. H. Bae, K. S. Lim, M. H. Jeong, C. Choi, S.-K. Choi, S. C. Kim and J.-W. Nah, *Macromol. Res.*, 2015, **23**, 237–244.
11 A. A. Shitole, P. S. Giram, P. W. Raut, P. P. Rade, A. P. Khandwekar, N. Sharma and B. Garnaik, *J. Biomater. Appl.*, 2019, **33**, 1327–1347.
12 N. Bricout, F. Chai, J. Sobocinski, A. Hertault, W. Laure, A. Ung, P. Woisel, J. Lyskawa and N. Blanchemain, *Mater. Sci. Eng., C*, 2020, **113**, 110967.
13 E.-M. Hietala, P. Maasilta, H. Juuti, J.-P. Nuutinen, A. L. Harjula, U.-S. Salminen and R. Lassila, *Thromb. Haemostasis*, 2004, **92**, 1394–1401.
14 S. J. Lee, H. H. Jo, K. S. Lim, D. Lim, S. Lee, J. H. Lee, W. D. Kim, M. H. Jeong, J. Y. Lim, I. K. Kwon, *et al.*, *Chem. Eng. J.*, 2019, **378**, 122116.
15 S. Meng, Z. Liu, L. Shen, Z. Guo, L. L. Chou, W. Zhong, Q. Du and J. Ge, *Biomaterials*, 2009, **30**, 2276–2283.
16 N. Huang, P. Yang, Y. Leng, J. Chen, H. Sun, J. Wang, G. Wang, P. Ding, T. Xi and Y. Leng, *Biomaterials*, 2003, **24**, 2177–2187.
17 R. Hou, L. Wu, J. Wang, Z. Yang, Q. Tu, X. Zhang and N. Huang, *Biomolecules*, 2019, **9**, 69.
18 J. Y. Park, C. H. Gemmell and J. E. Davies, *Biomaterials*, 2001, **22**, 2671–2682.
19 L. B. Koh, I. Rodriguez and S. S. Venkatraman, *Biomaterials*, 2010, **31**, 1533–1545.
20 R. Schieber, F. Lasserre, M. Hans, M. Fernández-Yagüe, M. Díaz-Ricart, G. Escolar, M.-P. Ginebra, F. Mücklich and M. Pegueroles, *Adv. Healthcare Mater.*, 2017, **6**, 1700327.
21 K. Zhang, T. Liu, J.-A. Li, J.-Y. Chen, J. Wang and N. Huang, *J. Biomed. Mater. Res., Part A*, 2014, **102**, 588–609.
22 P. Mulinti, J. Brooks, B. Lervick, J. Pullan and A. Brooks, *Hemocompatibility of Biomaterials for Clinical Applications*, Elsevier, 2018, pp. 253–278.
23 J. Zhao and Y. Feng, *Adv. Healthcare Mater.*, 2020, **9**, 2000920.
24 L. J. Taite, P. Yang, H.-W. Jun and J. L. West, *J. Biomed. Mater. Res., Part B*, 2008, **84**, 108–116.
25 S. Omar and A. de Belder, *Functionalised Cardiovascular Stents*, Elsevier, 2018, pp. 291–304.
26 N. Beshchasna, M. Saqib, H. Kraskiewicz, Ł. Wasyluk, O. Kuzmin, O. C. Duta, D. Ficai, Z. Ghizdavet, A. Marin, A. Ficai, *et al.*, *Pharmaceutics*, 2020, **12**, 349.
27 F. Boccafoschi, L. Fusaro and M. Cannas, *Functionalised Cardiovascular Stents*, Elsevier, 2018, pp. 305–318.
28 S. J. Lee, M. E. Kim, H. Nah, J. M. Seok, M. H. Jeong, K. Park, I. K. Kwon, J. S. Lee and S. A. Park, *J. Colloid Interface Sci.*, 2019, **537**, 333–344.
29 M. López-García and H. Kessler, *Handbook of Biomineralization: Biological Aspects and Structure Formation*, 2007, pp. 109–126.
30 H. Martin-Gómez, L. Oliver-Cervelló, I. Sánchez-Campillo, V. Marchán, M.-P. Ginebra and C. Mas-Moruno, *Chem. Commun.*, 2021, **57**, 982–985.
31 L. Oliver-Cervelló, H. Martin-Gómez, L. Reyes, F. Noureddine, E. Ada Cavalcanti-Adam, M.-P. Ginebra and C. Mas-Moruno, *Adv. Healthcare Mater.*, 2021, **10**, 2001757.
32 J. A. Hubbell, S. P. Massia, N. P. Desai and P. D. Drumheller, *Biotechnology*, 1991, **9**, 568.
33 I.-H. Bae, M. H. Jeong, D. S. Park, K. S. Lim, J. W. Shim, M. K. Kim and J.-K. Park, *Biomater. Res.*, 2020, **24**, 1–9.
34 M. I. Castellanos, C. Mas-Moruno, A. Grau, X. Serra-Picamal, X. Trepat, F. Albericio, M. Joner, F. J. Gil, M. P. Ginebra, J. M. Manero, *et al.*, *Appl. Surf. Sci.*, 2017, **393**, 82–92.
35 H. Aubin, C. Mas-Moruno, M. Iijima, N. Schütterle, M. Steinbrink, A. Assmann, F. J. Gil, A. Lichtenberg, M. Pegueroles and P. Akhyari, *Tissue Eng., Part C*, 2016, **22**, 496–508.
36 C. Mas-Moruno, R. Fraioli, F. Albericio, J. M. Manero and F. J. Gil, *ACS Appl. Mater. Interfaces*, 2014, **6**, 6525–6536.
37 M. Hoyos-Nogués, E. Falgueras-Batlle, M.-P. Ginebra, J. M. Manero, J. Gil and C. Mas-Moruno, *Int. J. Mol. Sci.*, 2019, **20**, 1429.
38 L. Oliver-Cervelló, H. Martin-Gómez, N. Mandakhbayar, Y.-W. Jo, E. A. Cavalcanti-Adam, H.-W. Kim, M.-P. Ginebra, J.-H. Lee and C. Mas-Moruno, *Adv. Healthcare Mater.*, 2022, **11**, 2201339.

39 V. Chausse, R. Schieber, Y. Raymond, B. Ségry, R. Sabaté, K. Kolandaivelu, M.-P. Ginebra and M. Pegueroles, *Addit. Manuf.*, 2021, 102392.
40 M. Amblard, J.-A. Fehrentz, J. Martinez and G. Subra, *Mol. Biotechnol.*, 2006, **33**, 239–254.
41 I. Coin, M. Beyermann and M. Bienert, *Nat. Protoc.*, 2007, **2**, 3247.
42 J. Kujawa, E. Rynkowska, K. Fatyeyeva, K. Knozowska, A. Wolan, K. Dzieszkowski, G. Li and W. Kujawski, *Polymers*, 2019, **11**, 1217.
43 K.-Y. Law and H. Zhao, *Surface Wetting*, Springer, 2016, pp. 135–148.
44 G. Ström, M. Fredriksson and P. Stenius, *J. Colloid Interface Sci.*, 1987, **119**, 352–361.
45 G. Arderiu, M. Díaz-Ricart, B. Buckley, G. Escolar and A. Ordinas, *Biochem. J.*, 2002, **364**, 65–71.
46 J. He, Q. Liu, S. Zheng, R. Shen, X. Wang, J. Gao, Q. Wang, J. Huang and J. Ding, *ACS Appl. Mater. Interfaces*, 2021, **13**, 42344–42356.
47 S. Lowe, N. M. O'Brien-Simpson and L. A. Connal, *Polym. Chem.*, 2015, **6**, 198–212.
48 S. Pacharra, S. McMahon, P. Duffy, P. Basnett, W. Yu, S. Seisel, U. Stervbo, N. Babel, I. Roy, R. Viebahn, *et al.*, *Front. Bioeng. Biotechnol.*, 2020, **8**, 991.
49 Y. Wan, J. Yang, J. Yang, J. Bei and S. Wang, *Biomaterials*, 2003, **24**, 3757–3764.
50 A. Shah, S. Shah, G. Mani, J. Wenke and M. Agrawal, *J. Tissue Eng. Regener. Med.*, 2011, **5**, 301–312.
51 R. Schieber, Y. Raymond, C. Caparrós, J. Bou, E. Herrero Acero, G. M. Guebitz, C. Canal and M. Pegueroles, *Appl. Sci.*, 2021, **11**, 1478.
52 Y. Lei, M. Rémy, C. Labrugère and M.-C. Durrieu, *J. Mater. Sci.: Mater. Med.*, 2012, **23**, 2761–2772.
53 R. Fraioli, S. Neubauer, F. Rechenmacher, B. Bosch, K. Dashnyam, J.-H. Kim, R. Perez, H.-W. Kim, F. Gil, M. Ginebra, *et al.*, *Biomater. Sci.*, 2019, **7**, 1281–1285.
54 M. Hoyos-Nogues, F. Velasco, M.-P. Ginebra, J. M. Manero, F. J. Gil and C. Mas-Moruno, *ACS Appl. Mater. Interfaces*, 2017, **9**, 21618–21630.
55 S. Noel, A. Hachem, Y. Merhi and G. De Crescenzo, *Biomacromolecules*, 2015, **16**, 1682–1694.
56 J. H. Lee, G. Khang, J. W. Lee and H. B. Lee, *J. Colloid Interface Sci.*, 1998, **205**, 323–330.
57 M. Pegueroles Neyra, *Interactions between titanium surfaces and biological components*, Universitat Politècnica de Catalunya, PhD thesis, 2009.
58 B. A. Butruk-Raszeja, M. S. Dresler, A. Kuźmińska and T. Ciach, *Colloids Surf., B*, 2016, **144**, 335–343.
59 M. Gabriel, K. Niederer, M. Becker, C. M. Raynaud, C.-F. Vahl and H. Frey, *Bioconjugate Chem.*, 2016, **27**, 1216–1221.
60 C. Wen, J. Zhang, Y. Li, W. Zheng, M. Liu, Y. Zhu, X. Sui, X. Zhang, Q. Han, Y. Lin, *et al.*, *Biomater. Sci.*, 2020, **8**, 5441–5451.
61 Y. Liu, M. C. Munisso, A. Mahara, Y. Kambe and T. Yamaoka, *Colloids Surf., B*, 2020, **193**, 111113.
62 R. Zhou, Y. Wu, K. Chen, D. Zhang, Q. Chen, D. Zhang, Y. She, W. Zhang, L. Liu, Y. Zhu, *et al.*, *Adv. Mater.*, 2022, **34**, 2200464.
63 W. S. Choi, Y. K. Joung, Y. Lee, J. W. Bae, H. K. Park, Y. H. Park, J.-C. Park and K. D. Park, *ACS Appl. Mater. Interfaces*, 2016, **8**, 4336–4346.
64 D. E. Anderson, K. P. Truong, M. W. Hagen, E. K. Yim and M. T. Hinds, *Acta Biomater.*, 2019, **86**, 291–299.
65 G. Peng, D. Yao, Y. Niu, H. Liu and Y. Fan, *Macromol. Biosci.*, 2019, **19**, 1800368.
66 C. W. Chung, H. W. Kim, Y. B. Kim and Y. H. Rhee, *Int. J. Biol. Macromol.*, 2003, **32**, 17–22.
67 A. Strohbach and R. Busch, *Int. J. Mol. Sci.*, 2021, **22**, 11390.
68 E. Y. Kang, S.-B. Park, B. Choi, S.-W. Baek, K.-W. Ko, W.-K. Rhim, W. Park, I.-H. Kim and D. K. Han, *Biomater. Sci.*, 2020, **8**, 2018–2030.
69 A. Strohbach, F. Maess, K. Wulf, S. Petersen, N. Grabow, K.-P. Schmitz, S. B. Felix and R. Busch, *Int. J. Mol. Sci.*, 2021, **22**, 6340.
70 G. Apte, A. Lindenbauer, J. Schemberg, H. Rothe and T.-H. Nguyen, *ACS Omega*, 2021, **6**, 10963–10974.
71 M. Szymonowicz, Z. Rybak, W. Witkiewicz, C. Pezowicz and J. Filipiak, *Acta Bioeng. Biomech.*, 2014, **16**, 131–139.
72 Y. Ramot, M. Haim-Zada, A. J. Domb and A. Nyska, *Adv. Drug Delivery Rev.*, 2016, **107**, 153–162.
73 K. Bastekova, O. Guselnikova, P. Postnikov, R. Elashnikov, M. Kunes, Z. Kolska, V. Švorčík and O. Lyutakov, *Appl. Surf. Sci.*, 2017, **397**, 226–234.
74 R. Khalifehzadeh, W. Ciridon and B. D. Ratner, *Acta Biomater.*, 2018, **78**, 23–35.
75 L. Zhang, B. Casey, D. K. Galanakis, C. Marmorat, S. Skoog, K. Vorvolakos, M. Simon and M. H. Rafailovich, *Acta Biomater.*, 2017, **54**, 164–174.
76 K. Nguyen, S.-H. Su, A. Sheng, D. Wawro, N. Schwade, C. Brouse, P. Greilich, L. Tang and R. Eberhart, *Biomaterials*, 2003, **24**, 5191–5201.
77 A. Gao, F. Liu and L. Xue, *J. Membr. Sci.*, 2014, **452**, 390–399.
78 Z. Xiong, F. Liu, H. Lin, J. Li and Y. Wang, *ACS Biomater. Sci. Eng.*, 2016, **2**, 2207–2216.
79 K. Kim, S. Park, J. H. Park, W.-S. Cho, H.-E. Kim, S.-M. Lee, J. E. Kim, H.-S. Kang and T.-S. Jang, *J. Korean Neurosurg. Soc.*, 2021, **64**, 853–863.
80 A. Rudolph, M. Teske, S. Illner, V. Kiefel, K. Sternberg, N. Grabow, A. Wree and M. Hovakimyan, *PLoS One*, 2015, **10**, e0142075.
81 M. I. Castellanos, J. Guillem-Marti, C. Mas-Moruno, M. Díaz-Ricart, G. Escolar, M. P. Ginebra, F. J. Gil, M. Pegueroles and J. M. Manero, *J. Biomed. Mater. Res., Part A*, 2017, **105**, 973–983.
82 N. N. Tandon, E. A. Holland, U. Kralisz, H. K. Kleinman, F. Robey and G. Jamieson, *Biochem. J.*, 1991, **274**, 535–542.
83 B. Sivaraman and R. A. Latour, *Biomaterials*, 2011, **32**, 5365–5370.
84 T. G. Kapp, F. Rechenmacher, S. Neubauer, O. V. Maltsev, E. A. Cavalcanti-Adam, R. Zarka, U. Reuning, J. Notni, H.-J. Wester, C. Mas-Moruno, *et al.*, *Sci. Rep.*, 2017, **7**, 39805.